Conjugation of Disassembled Zincphthalocyanine-based Nanocomposites and the Synergistic Effect on Visible-light Photosensitive Activity①

ZHAO Wen-Bo ZHANG Ya-Lan
XU Guang-Yu JIA Xiao② XUE Jin-Ping②
(*National & Local Joint Biomedical Engineering Research Center on Photodynamic Technologies, College of Chemistry, Fuzhou University, Fuzhou* 350116, *China*)

ABSTRACT In this research, a conjugated Pc-MIL-88B (Fe) nanoplatform was constructed via a condensation process between modified zinc phthalocyanine and MIL-88B (Fe) for the removal of organic pollutants. The as-prepared material was fully characterized by TEM, XPS, ICP, FTIR, UV-Vis, N_2 adsorption-desorption isotherm, etc. The results indicate that Pc-MIL-88B (Fe) preserved the topological structure of MIL-88B (Fe), and the micropores of framework could effectively prevent the aggregation of Pc in water. Meanwhile, the conjugated Pc-MIL-88B (Fe) basically maintains the singlet oxygen quantum yield of Pc, and behaves a much higher photocurrent intensity compared to NH_2-MIL-88B (Fe). Additionally, the photosensitive activity and reusability of Pc-MIL-88B (Fe) were evaluated by the degradation of methylene blue in aqueous solution under visible light irradiation, and the degradation mechanism was also investigated in detail.

Keywords: metal-organic frameworks, zinc phthalocyanine, photosensitive activity, synergistic effect;
DOI: 10.14102/j.cnki.0254–5861.2011–3104

1 INTRODUCTION

With the continuous development of industry, more and more attention has been paid to the environmental problems caused by industrial wastewater, seriously endangering human health[1, 2]. The photosensitive oxidation technology that oxidizes the structure of pollutants into environmentally friendly substances via photoinduced degradation should be an effective treatment[3, 4]. As an important part of photosensitive materials, photosensitive inorganic semiconductors have been widely used in degrading pollutants due to their safety and non-toxic advantages[5]. However, inorganic semiconductor material usually has wide band gap, and can only absorb ultraviolet light but little visible light, which limits its practical application[6, 7].

As a typical organic semiconductor, metalphthalocyanine with a planar conjugated structure of 18π electrons has wide and outstanding visible light response, and the radical and radical anions produced by visible light irradiation make it exhibit photodynamic activity. However, the inevitable π-π stacking causes metalphthalocyanine molecules to aggregate in the solvents, which would lead to an unexpected decrease of photosensitive activity[8-10].

Fortunately, phthalocyanine molecules have the advantage of being easy to modify, and can be functionalized by introducing different substituents to their benzene ring[11-13], which provides an effective method for reducing the aggregation. Hence, the construction of suitable nanocarriers that can conjugate with functionalized phthalocyanine to improve its aggregation is highly desired.

Metal-organic frameworks (MOFs) as promising porous materials are constructed by metal ions or metal ion clusters and organic ligands. MOFs have large specific surface area, high porosity and plentiful active sites, and can be conveniently adjusted and functionalized according to the desired properties, which play an important role in functional areas, such as in catalysis, gas sensing, drug delivery, etc[14, 15]. Thereinto, as an iron-containing MOF, MIL-88B (Fe) has

Received 20 January 2021; accepted 8 April 2021
① The work was supported by the National Health and Family Planning Commission jointly established Scientific Research Fund (No. WKJ2016-2-14) and the Natural Science Foundation of Fujian Province (No. 2017J05021)
② Corresponding authors. E-mail: jiaxiao@fzu.edu.cn and xuejinping66@fzu.edu.cn

attracted broad attention owing to its incorporation with semiconductor character and Fenton process[16]. Meanwhile, the good water stability and visible light absorption characteristic caused by Fe_3-μ_3-oxo clusters endow it with outstanding advantages distinguished from most other MOFs[17, 18]. As a result, it will be worthwhile to develop MIL-88B (Fe) as an effective photosensitizing material as well as a nanoscale scaffold.

Establishing a stable connection between the photosensitizer and the metal-organic framework will help ensure the yield of singlet oxygen during the photosensitization process and prevent the photosensitizer from leaking in advance[19, 20]. In this work, we present a facile approach for the synthesis of Pc-MIL-88B (Fe) via covalent conjugation. The topological structure of MIL-88B (Fe) could maximize its relatively dispersed active sites, and its functionalization and further conjugation will be beneficial to inhibit the aggregation and thus keep the monomeric state of Pc in water. In addition, the constructed nano-platform combines the advantages of visible light response of Pc and MIL-88B(Fe), and the final synergistic effect makes it exhibit high photosensitive activity as expected.

2 EXPERIMENTAL

2. 1 Chemicals

Methylparaben, 4-nitrophthalonitrile, anhydrous potassium carbonate (K_2CO_3), anhydrous zinc acetate ($Zn(OAc)_2$), 1,8-diazabicyclo (5.4.0) undec-7-ene (DBU), sodium hydroxide (NaOH), N,N-dimethylformamide (DMF), *n*-pentanlol, methanol, tetrahydrofuran (THF), ethanol, pluronic F127 ($EO_{97}PO_{69}EO_{97}$, with an average Mn = 12600, Aldrich), $FeCl_3$ $6H_2O$ (Aldrich, 97%), acetic acid (CH_3COOH, 99.7%), 2-aminoterephthalic acid (NH_2-BDC N-(3-dimethylaminopropyl)-N′-ethylcarbodiimide hydrochloride (EDCI) and 1-hydroxy-benzotriazole monohydrate (HOBT H_2O).

2. 2 Synthesis of 4-[4-(methoxycarbonyl) phenoxy]phthalonitrile

4-Nitrophthalonitrile (0.97 g) and methylparaben (0.87 g) were added in 20 mL of anhydrous DMF. After stirring until the mixture dissolved, anhydrous K_2CO_3 (1.38 g) was added. The above solution was stirred at room temperature for 12 h under N_2 atmosphere. After reaction, the ice-water was poured into the system and stirred thoroughly. The suspension was first filtered through a Buchner funnel, and the obtained residue was recrystallized by ethanol, then the final white powder product 4-[4-(methoxycarbonyl) phenoxy]phthalonitrile was gained via further filtration using a Buchner funnel[21, 22].

2. 3 Synthesis of zinc(II) 2,9(10),16(17),23(24)-tetrakis[4-(methoxycarbonyl)phenoxy]phthalocyanine

4-[4-(Methoxycarbonyl)phenoxy]phthalonitrile (1.28 g) was dissolved in 30 mL anhydrous *n*-pentanlol, and stirred in an oil bath at 100 ℃ under N_2 atmosphere. After the reaction solution was clarified, anhydrous zinc acetate (0.4 g) and DBU (0.7 mL) were added, and then the temperature was raised to 135 ℃ for overnight reaction. The solvent was removed in vacuum, and the collected residue was ultrasonically washed *via* adding a certain amount of methanol. The obtained suspension was filtered through a Buchner funnel, and the final blue-green product was further purified by silica gel column using CH_2Cl_2/CH_3OH (20:1) as the eluent to obtain zinc(II) 2,9(10),16(17),23(24)-tetrakis-[4-(methoxycarbonyl)phenoxy]phthalocyanine[23, 24].

2. 4 Synthesis of zinc(II) 2,9(10),16(17),23(24)-tetrakis(4-carboxylphenoxy)phthalocyanine

Zinc(II) 2,9(10),16(17),23(24)-tetrakis[4-(methoxycarbonyl)phenoxy]phthalocyanine (0.50 g) was dissolved in THF (15 mL), and 100 mL methanol was added. Then 20 mL of pre-configured saturated NaOH solution was added, and the temperature of the oil bath was raised to 50 ℃ for overnight reaction. After the reaction was completed, the solvent was removed in vacuum, and 200 mL of deionized water was added, and the solution was filtered by dialysis membrane. Then the obtained filtrate was put into a beaker and 1 M hydrochloric acid was added, until no solid was precipitated. The suspension was filtered by dialysis membrane, and the final solid product was zinc(II) 2,9(10),16(17),23(24)-tetrakis(4-carboxylphenoxy)phthalocyanine (Pc)[25, 26]. The H^1NMR and Mass spectra are shown in Fig. S2 and S3.

2. 5 Synthesis of NH_2-MIL-88B (Fe)

NH_2-MIL-88B (Fe) product was synthesized via a hydrothermal method[27, 28]. Typically, 0.160 g F127 was first dissolved in 13 mL deionized water, and then 0.178 g $FeCl_3$ $6H_2O$ in 2 mL deionized water was added and stirred for 1 h. After 0.3 mL CH_3COOH was injected to the above mixture and stirred for another 1 h, 60 mg NH_2-BDC was added. The reaction mixture was stirred for 2 h, and then transferred into a Teflon-lined stainless-steel autoclave and heated at 110 ℃ for 24 h. The product was obtained via centrifugation and washed with anhydrous ethanol and DMF

for several times.

2. 6 Synthesis of Pc-MIL-88B (Fe)

Pc (30 mg) was dissolved in 10 mL DMF. EDCI (8.5 mg) and HOBT (6.0 mg) were dissolved in another 1.0 mL DMF, and the mixture was added to the previous solution. The final mixture was stirred at 0 ℃ for 30 min. 0.5 mL of triethylamine was added after the ice bath was removed, and 20 mg of NH_2-MIL-88B (Fe) was added after the reaction system was restored to room temperature. The reaction mixture was stirred for overnight. After reaction, the product was washed with DMF and ethanol for three times, and then collected by centrifuge.

2. 7 Characterization

The crystal phases of the products were detected by X-ray diffractometer (Rigaku D/Max 2200 PC). The morphology and microstructure were observed using high-resolution TEM (Tecnai G2 F20, FEI). The FTIR measurements were conducted on the VERTEX 70/70v FT-IR spectrometer. Fluorescence spectra were obtained on the FLS920 fluorescence spectrometer. UV-Vis absorption spectra experiments were performed by TU-1901 UV spectrometer. ^{1}H NMR spectra were recorded on BRUKER AVANCE III 400 (^{1}H, 400 MHz) in $CDCl_3$.

2. 8 Detection of singlet oxygen by DPBF assay

DPBF (1,3-diphenylisobenzofuran) assay method was used to measure the singlet oxygen production via the ultraviolet absorption intensity at 415 nm peak[29, 30]. The respective DMSO solution of unsubstituted ZnPc, H_4Pc, or Pc-MIL-88B (Fe) was thoroughly mixed with DPBF and transferred into a cuvette. Then the DMSO mixture solution was irradiated with a 670 nm light laser, and the absorption of DPBF at 415 nm was recorded every 1 min, ending up to 15 min.

2. 9 Evaluation of the photosensitive activity

The photosensitive activity was tested via the degradation of methylene blue (MB) under visible light irradiation ($\lambda > 420$ nm). Briefly, MB solution (50 mL, 2×10^{-5} M) and 10 mg of respective Pc, Pc-MIL-88B (Fe) or NH_2-MIL-88B (Fe) were first ultra-sounded for 2 min, and then stirred in the dark for 30 min to reach the adsorption-desorption dynamic equilibrium. The suspension was irradiated under visible light, and 3 mL of the reaction solution was collected at a certain interval (every interval of 10 min within the initial 30 min, while 30 min from 30 to 120 min) to obtain absorption value of the solution measured by UV-vis spectrophotometer.

3 RESULTS AND DISCUSSION

Fig. 1e shows the XRD patterns of the as-prepared NH_2-MIL-88B (Fe), Pc-MIL-88B (Fe) and the simulated data of NH_2-MIL-88B (Fe)[31]. The diffraction peaks of NH_2-MIL-88B (Fe) match well with the simulated NH_2-MIL-88B (Fe) single crystal, exhibiting pure product was synthesized. The characteristic diffraction peaks of Pc-MIL-88B (Fe) are also in good agreement with NH_2-MIL-88B (Fe), and no obvious peaks from pure Pc crystal can be observed. The results may indicate that the Pc molecules are relatively lower in content and dispersed in the micropores of NH_2-MIL-88B (Fe) rather than aggregation[32]. Moreover, the covalently bonded Pc molecules have no significant effect on the crystal structure of the as-synthesized Pc-MIL-88B (Fe). The colors of the synthetic product dispersed in DMF were brown, blue and green for NH_2-MIL-88B (Fe), Pc and Pc-MIL-88B (Fe), respectively (Fig. 1f). As all the products were re-dispersed after three times by centrifugation, the supernatant of Pc-MIL-88B (Fe) was basically colorless, which proves Pc has been successfully bonded to NH_2-MIL-88B (Fe).

The morphologies and micropores of NH_2-MIL-88B (Fe) and Pc-MIL-88B (Fe) were also investigated by SEM and TEM. As illustrated in Fig. 1a and 1b, NH_2-MIL-88B (Fe) exhibits uniform spindle-shape with sizes of ca. 200 nm in length and 40 nm in width. The spindle-shape morphology and particle size of NH_2-MIL-88B (Fe) have basically retained after the covalent modification of Pc, and no obvious aggregation of Pc can be observed in Fig. 1c and 1d. This indicates that the morphology of NH_2-MIL-88B (Fe) is almost unaffected by introducing Pc molecules into the structure, and the chemical bond between NH_2-MIL-88B (Fe) and Pc may be formed. The average hydrodynamic diameters of NH_2-MIL-88B (Fe) and Pc-MIL-88B (Fe) were 235.8 and 241.6 nm, according to the dynamic light scattering measurement (DLS) results in Fig. S1 and Table S1. The small size difference between NH_2-MIL-88B (Fe) and Pc-MIL-88B (Fe) further indicates that the bonded Pc does not have a significant impact on the size of NH_2-MIL-88B (Fe).

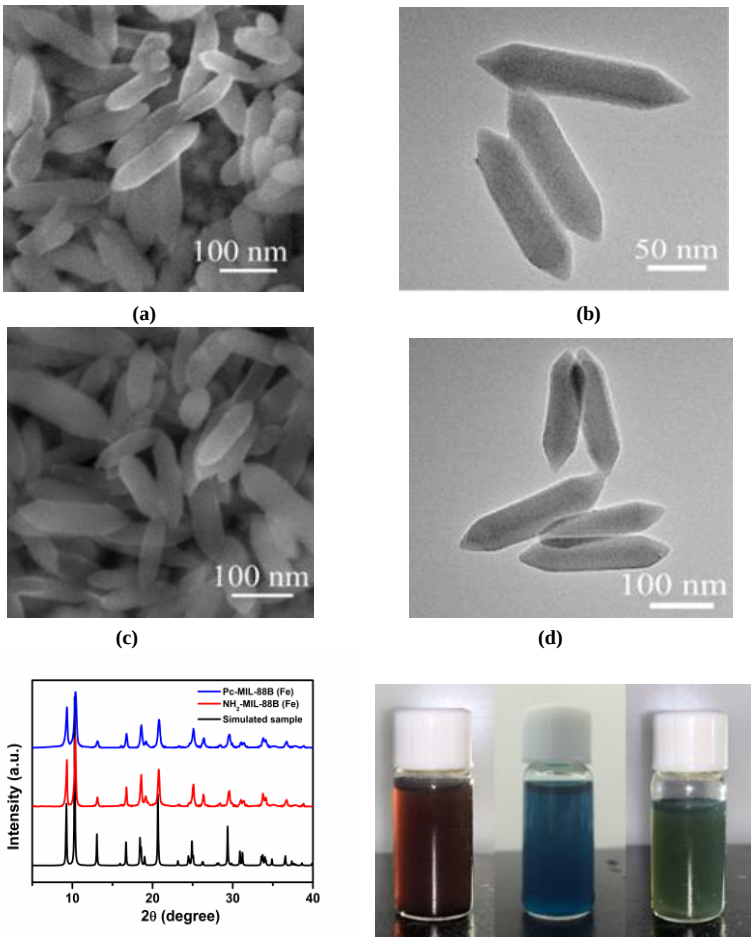

Fig. 1. SEM and TEM images of NH_2-MIL-88B (Fe) (a, b) and Pc-MIL-88B (Fe) (c, d). The corresponding XRD patterns (e), and the optical photographs of NH_2-MIL-88B (Fe), Pc and Pc-MIL-88B (Fe) in DMF (f)

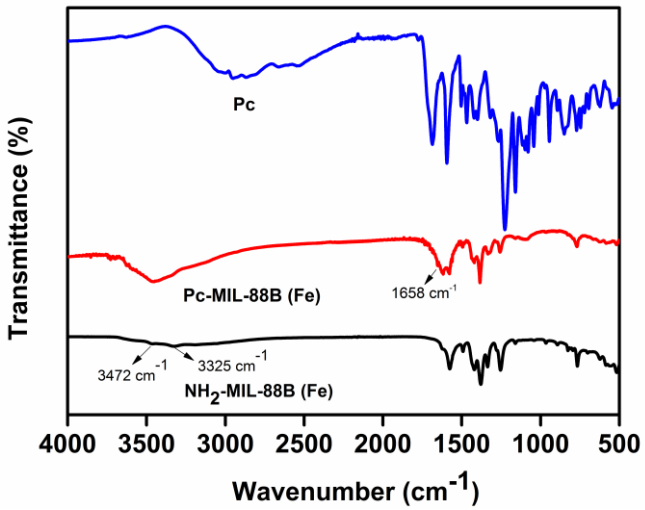

Fig. 2. FTIR spectra of the as-prepared Pc, NH_2-MIL-88B (Fe) and Pc-MIL-88B (Fe)

FT-IR and XPS spectra were further carried out to analyze the chemical structures of as-prepared NH_2-MIL-88B (Fe) and Pc-MIL-88B (Fe). As shown in Fig. 2, the bands at 3325 and 3472 cm^{-1} in NH_2-MIL-88B (Fe) can be attributed to the symmetric and asymmetric stretching vibrations of N–H bond, indicating the successful synthesis of amine groups[1, 33, 34]. After the modification of Pc, the two characteristic absorption peaks ascribed to the carboxyl group of Pc and the amino

group of NH_2-MIL-88B (Fe) basically disappeared, and a new small peak at 1658 cm^{-1} resulting from the carbonyl group appeared, revealing the existence of amination reaction between Pc and NH_2-MIL-88B (Fe)[35, 36].

As seen in Fig. 3, the as-prepared NH_2-MIL-88B (Fe) has no absorption peak in the range of 500～750 nm, and Pc behaved the characteristic absorption of phthalocyanine monomer at 611 and 680 nm in DMF[15]. For Pc-MIL-88B (Fe), the two characteristic absorption peaks of phthalocyanine still exist, which demonstrated the successful conjugation of Pc to NH_2-MIL-88B (Fe).

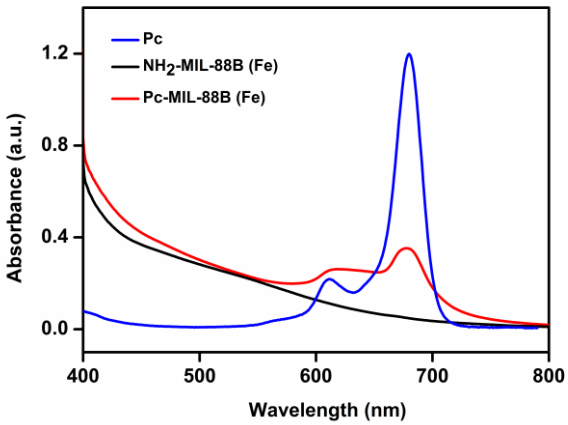

Fig. 3. UV-Vis absorption spectra of Pc, NH_2-MIL-88B (Fe) and Pc-MIL-88B (Fe) in DMF

Inductively coupled plasma mass spectrometer (ICP-MS) was used to quantify the loaded Pc in Pc-MIL-88B (Fe). The final specific amount of Pc was calculated via analyzing the zinc content in Pc-MIL-88B (Fe)[37]. According to the analysis result in Table S2, the mass fraction of Pc in Pc-MIL-88B (Fe) is approximately 3.2%.

Fig. S4 displays the nitrogen adsorption-desorption isotherms and the corresponding pore size distribution curve of the product. In Table S3, the specific surface areas of NH_2-MIL-88B (Fe) and Pc-MIL-88B (Fe) analyzed by the BET method were 62.71 and 50.10 m^2/g, respectively. The pore-size distribution of Pc-MIL-88B (Fe) calculated from the desorption branch by BJH method indicates a narrow distribution centered at ca. 1.70 nm. This demonstrates that after the amidation of Pc with NH_2-MIL-88B (Fe), the Pc-MIL-88B (Fe) still maintains a relative high specific surface area, and the covalent conjugation of Pc has little effect on the pore characteristics of the original MOF material. It will be beneficial to maintain the monomer state of Pc by using the microporous structure of NH_2-MIL-88B (Fe) in aqueous solution, and the photosensitive activity should be further improved as a result of the depolymerized Pc.

XPS analyses were used to determine the chemical environment and the specific elements in NH_2-MIL-88B (Fe) and Pc-MIL-88B (Fe). The survey scanning spectra in Fig. 4a reveal the presence of C, N, O, Fe and Zn in Pc-MIL-88B (Fe)[38]. In Fig. 4f, the Zn 2*p* peaks at 1021.7 and 1044.8 eV of Pc-MIL-88B (Fe) indicated that Pc has been successfully bonded to NH_2-MIL-88B (Fe)[39]. The two major peaks at 711.9 and 725.7 eV with the satellite peak at 717.8 eV of NH_2-MIL-88B (Fe) can be ascribed to binding energies of Fe $2p_{3/2}$, Fe $2p_{1/2}$ and the characteristic peak of Fe^{3+} (Fig. 4e), respectively. For Pc-MIL-88B (Fe), the partial peaks produced a slight negative displacement and shifted to 717.6 and 725.5 eV, which should be caused by the enhancement of electron density on Fe^{3+} and can further confirm the close contact between Pc and NH_2-MIL-88B (Fe).

The ability to generate reactive oxygen species can reflect the photosensitive activity of the material. The singlet oxygen quantum yield of the product is mainly affected by the following factors, the aggregation state of the photosensitizer, the quantum yield, energy level and lifetime of T1 (excited triplet state of photosensitizer), etc[40, 41]. To evaluate the photosensitizing efficiency of the as-prepared Pc-MIL-88B (Fe), the photoinduced production of $^1O_2$ was tested via the bleaching of 1,3-diphenylisobenzofuran (DPBF), which was used as an $^1O_2$ quencher[30, 42]. As shown in Fig. 5, the singlet oxygen quantum yield Φ_Δ of standard unsubstituted ZnPc is 0.56[29], while that of the as-prepared Pc and Pc-MIL-88B (Fe) is 0.558 and 0.574, respectively. The result indicates that the singlet oxygen quantum yield of Pc can be

maintained after being covalently connected with NH_2-MIL-88B (Fe), showing the good ability of producing $^1O_2$ of Pc-MIL-88B (Fe).

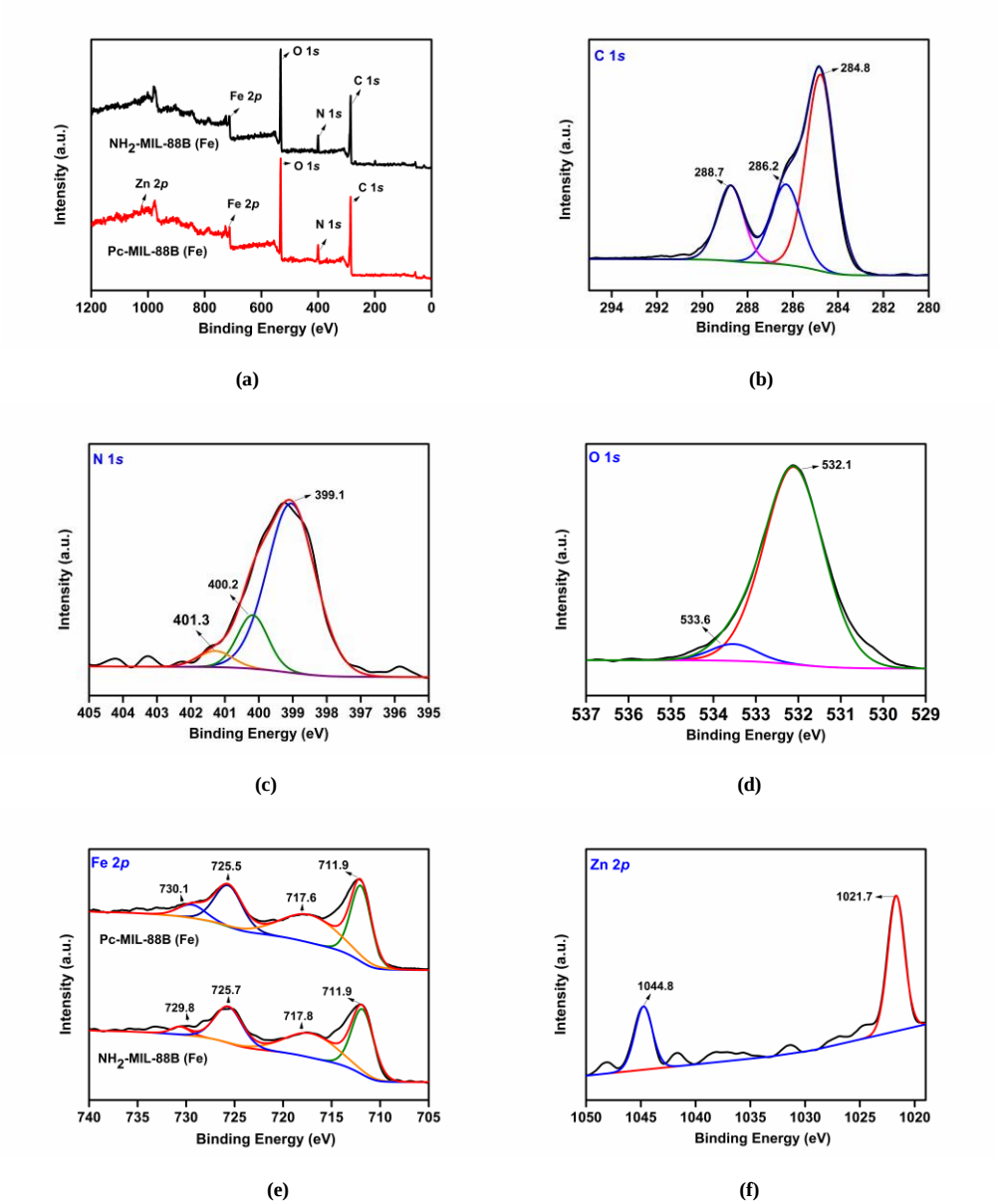

Fig. 4. XPS spectra of Pc-MIL-88B (Fe) (a) Wide spectra, (b) C 1*s*, (c) N 1*s*, (d) O 1*s*, (e) Fe 2*p*, (f) Zn 2*p*

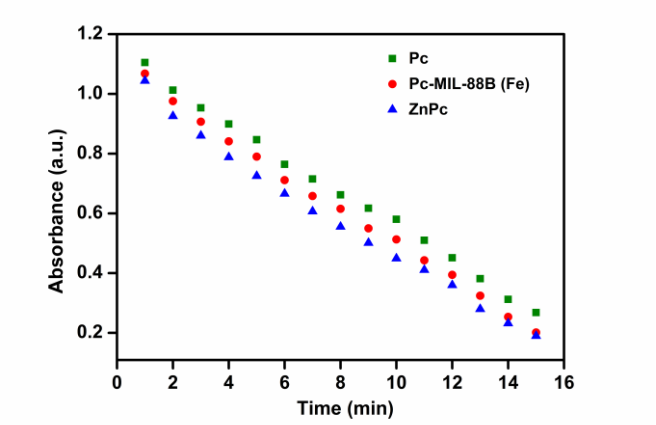

Fig. 5. Singlet oxygen generation test for the synthesized Pc and Pc-MIL-88B (Fe) with using unsubstituted ZnPc as the reference in DMF

Fig. 6a shows the transient photocurrent response curves generated by NH_2-MIL-88B (Fe) and Pc-MIL-88B (Fe) under intermittent exposure to visible light. As can be seen, when the material is exposed to intermittent illumination of light, the corresponding photocurrent response value rose rapidly for both NH_2-MIL-88B (Fe) and Pc-MIL-88B (Fe). But in comparison, it is obvious that the photocurrent intensity of Pc-MIL-88B (Fe) is much higher than that of NH_2-MIL-88B (Fe) (ca. 10 times). The result means Pc-MIL-88B (Fe) has higher sensitivity and utilization of visible light, which should be attributed the synergistic effect between Pc that produces reactive oxygen species and the Fenton activity of NH_2-MIL-88B (Fe). Hence, more photo carriers and efficient charge transfer would be generated, and ultimately improves the photosensitive properties of Pc-MIL-88B (Fe)[43, 44].

The cyclic voltammetry curves of NH_2-MIL-88B (Fe) and Pc-MIL-88B (Fe) are shown in Fig. 6b. It is found that Pc-MIL-88B (Fe) exhibits higher peak currents than NH_2-MIL-88B (Fe), which proved the higher REDOX capacity of Pc-MIL-88B (Fe). Compared with NH_2-MIL-88B (Fe), a new pair of REDOX peaks was observed in Pc-MIL-88B (Fe), which was the reduction peak at –0.1 V and the widened oxidation peak at ca. 0.4 V. The broadening peak may be related to the superposition of the oxidation peak after modification of Pc. The higher REDOX capacity and new electro-catalysis reaction in Pc-MIL-88B (Fe) would be beneficial to improve its photosensitive activity[45].

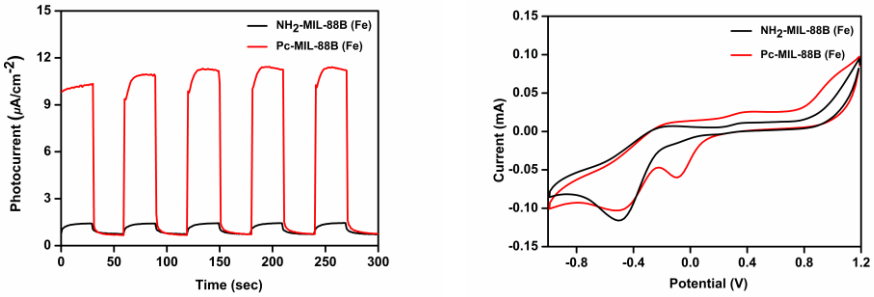

(a) **(b)**

Fig. 6. Transient photocurrent response (a) and cyclic voltammetry curves (b) of NH_2-MIL-88B (Fe) and Pc-MIL-88B (Fe)

The photosensitive efficiency of Pc-MIL-88B (Fe) was evaluated by the degradation of MB solution under visible light, while using NH_2-MIL-88B (Fe) or Pc for comparison[46, 47]. When only Pc was added, MB basically maintained the initial concentration without degradation. This result shows that the addition of Pc does not have obvious photosensitive degradation activity for MB, which could be attributed to the aggregation of Pc in water. When only NH_2-MIL-88B (Fe) was added, the removal effect of MB can only be achieved to 40.2% after 120 min. Compared with single NH_2-MIL-88B (Fe) or Pc, the degradation efficiency of Pc-MIL-88B (Fe) reached 91% (Fig. 7a). The significantly higher removal ratio of Pc-MIL-88B (Fe) should be attributed to the disaggregation of Pc conjugated with NH_2-MIL-88B (Fe) in micropores, which improves its exposure to oxygen and meanwhile enhances the synergistic effect of the two components.

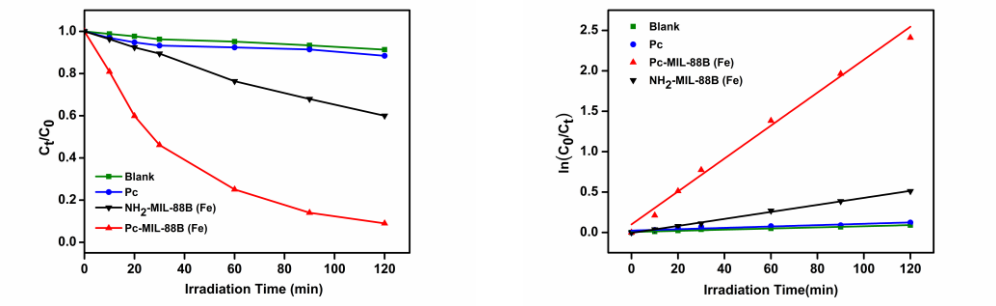

(a) **(b)**

Fig. 7. Photosensitive curves (a) and the corresponding pseudo-first-order kinetics curves (b) of MB degradation under visible light irradiation

As shown in Fig. 7b, the chart of the natural logarithm of C_t/C_0 of MB versus irradiation time with adding different materials performs their respective linear fit. The calculated slope was described as the reaction rate constant (k) in the quasi-first-order mode. The slope of Pc-MIL-88B (Fe) with a k value of 0.0203 min^{-1} was obviously higher than that of the other materials, indicating its prominent photosensitive degradation effect on MB solution[25].

The reusability is an important parameter for the photo-sensitized materials[48]. As a result, a cyclic degradation experiment of MB was performed to investigate the reusability of the as-prepared Pc-MIL-88B (Fe). As shown in Fig. 8, the photosensitive efficiency of Pc-MIL-88B (Fe) can still be maintained above 85% after 3rd cycle for degradation of MB, which indicates that the prepared material has good stability and can be reused to avoid secondary damage to the environment.

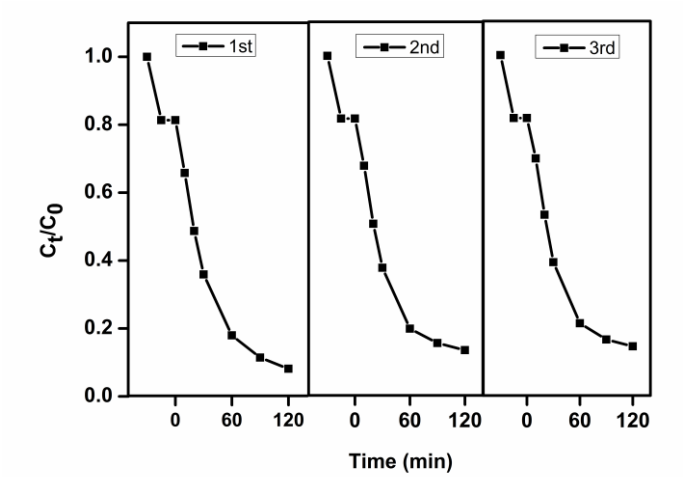

Fig. 8. Recycle experiments of MB degradation by Pc-MIL-88B (Fe) during three cycles

In order to explore the degradation mechanism of Pc-MIL-88B (Fe) under visible light, the experiment was conducted by adding different scavengers[49, 50]. According to the active species that may be generated during degradation, EDTA-2Na, BQ and IPA were used to capture electron-hole (h^+), superoxide anion (O_2^-), and hydroxyl free Radical (OH)[51, 52], respectively. In Fig. 9, the degradation efficiency was decreased to varying degrees after adding scavengers. Thereinto, when EDTA-2Na was added, the degradation efficiency of MB was reduced from 91% to 42%, which indicates that the photo-generated holes should be the main active species involved in the photosensitive process. The previous experiments have confirmed the high singlet oxygen quantum yield of the as-prepared Pc-MIL-88B (Fe), so the prominent degradation activity should be ascribed to both photosensitive mechanisms I and II[53].

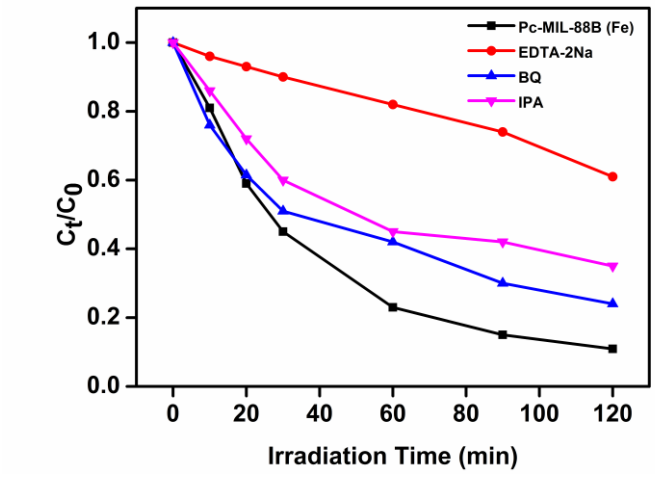

Fig. 9. Photosensitive efficiency of MB on Pc-MIL-88B (Fe) with different scavengers

4 CONCLUSION

In summary, Pc-MIL-88B (Fe) was synthesized by the covalent connection of the hydrophobic photosensitizer Pc and the metal organic framework NH_2-MIL-88B (Fe). The well-defined porous structure of MIL-88B (Fe) substantially improves the aggregation of Pc in water, which has a decisive influence on the final photosensitivity of the product. The as-prepared Pc-MIL-88B (Fe) nanoplatform presents good stability, high transient photocurrent response, and satisfied singlet oxygen quantum yield. The excellent visible-light photosensitive efficiency of Pc-MIL-88B (Fe) for MB indicated the synergistic effect of Pc and MIL-88B (Fe), which makes it great prospects for application in environmental treatment field.

REFERENCES

(1) Li, Q.; Wang, H. G.; Li, Y.; Li, Y.; Duan, Q. Conjugated microporous polymers bearing metallophthalocyanine moieties with enhanced visible-light photocatalytic activity. *Dyes Pigments.* **2018**, 149, 261–267.

(2) Yang, W. L.; Liu, G. S.; Chen, Y. H.; Miao, D. T.; Wei, Q. P.; Li, H. C.; Ma, L.; Zhou, K. C.; Liu, L. B.; Yu, Z. M. Persulfate enhanced electrochemical oxidation of highly toxic cyanide-containing organic wastewater using boron-doped diamond anode. *Chemosphere* **2020**, 252, 126499–10.

(3) Wang, J. H.; Shao, X. Z.; Liu, J. H.; Zhang, Q.; Ji, X. H.; Tian, G. H. Mesoporous magnetic *g*-C_3N_4 nanocomposites for photocatalytic environmental remediation under visible light. *Ecotoxicol. Environ. Saf.* **2020**, 205, 111147–9.

(4) Wu, M. X.; Lei, H.; Chen, J. Y.; Dong, X. P. Friction energy harvesting on bismuth tungstate catalyst for tribocatalytic degradation of organic pollutants. *J. Colloid Interface Sci.* **2021**, 587, 883–890.

(5) Cai, T.; Liu, Y. T.; Wang, L. L.; Zhang, S. Q.; Zeng, Y. X.; Yuan, J. J.; Ma, J. H.; Dong, W. Y.; Liu, C. B.; Luo, S. L. Silver phosphate-based Z-scheme photocatalytic system with superior sunlight photocatalytic activities and anti-photocorrosion performance. *Appl. Catal. B* **2017**, 208, 1–13.

(6) Mohanta, M. K.; Kishore, A.; De Sarkar, A. Two-dimensional ultrathin van der waals heterostructures of indium selenide and boron monophosphide for superfast nanoelectronics, excitonic solar cells, and digital data storage devices. *Nanotechnology* **2020**, 31, 495208–16.

(7) Yu, J. C.; Xie, Y.; Tang, H. Y.; Zhang, L.; Chan, H. C.; Zhao, J. Visible light-assisted bactericidal effect of metalphthalocyanine-sensitized titanium dioxide films. *J. Photochem. Photobiol. A* **2003**, 156, 235–241.

(8) Ding, X.; Han, B. H. Metallophthalocyanine-based conjugated microporous polymers as highly efficient photosensitizers for singlet oxygen generation. *Angew. Chem. Int. Edit.* **2015**, 54, 6536–9.

(9) Mgidlana, S.; Nyokong, T. Photocatalytic desulfurization of dibenzothiophene using asymmetrical zinc(II) phthalocyanines conjugated to silver-magnetic nanoparticles. *Inorg. Chim. Acta* **2021**, 514, 119970–12.

(10) Thakur, N. S.; Mandal, N.; Patel, G.; Kirar, S.; Reddy, Y. N.; Kushwah, V.; Jain, S.; Kalia, Y. N.; Bhaumik, J.; Banerjee, U. C. Co-administration of zinc phthalocyanine and quercetin via hybrid nanoparticles for augmented photodynamic therapy. *Nanomed.-Nanotechnol. Biol. Med.* **2021**, 33, 102368–12.

(11) Peng, J. Y.; Wei, L. Y.; Liu, Y. X.; Zhuge, W. F.; Huang, Q.; Huang, W.; Xiang, G.; Zhang, C. Z. Novel porous iron phthalocyanine based metal-organic framework electrochemical sensor for sensitive vanillin detection. *RSC Adv.* **2020**, 10, 36828–36835.

(12) Yuan, Z. C.; Lan, Y.; Chen, S. Y.; Chen, D. J. Preparation of magnetically recyclable palygorskite Fe-octacarboxylic acid phthalocyanine nano-composites and their photocatalytic behavior for degradation of Rhodamine B. *Appl. Clay Sci.* **2017**, 147, 153–159.

(13) Wong, R. C. H.; Lo, P. C.; Ng, D. K. P. Stimuli responsive phthalocyanine-based fluorescent probes and photosensitizers. *Coord. Chem. Rev.* **2019**, 379, 30–46.

(14) Wan, S. S.; Cheng, Q.; Zeng, X.; Zhang, X. Z. A Mn(III)-sealed metal-organic framework nanosystem for redox-unlocked tumor theranostics. *ACS Nano* **2019**, 13, 6561–6571.

(15) Deng, Q. Q.; Sun, P. P.; Zhang, L.; Liu, Z. W.; Wang, H.; Ren, J. S.; Qu, X. G. Porphyrin MOF dots-based, function-adaptive nanoplatform for enhanced penetration and photodynamic eradication of bacterial biofilms. *Adv. Funct. Mater.* **2019**, 29, 1903018–9.

(16) Liu, X. C.; Zhou, Y. Y.; Zhang, J. C.; Tang, L.; Luo, L.; Zeng, G. M. Iron containing metal-organic frameworks: structure, synthesis, and applications in environmental remediation. *ACS Appl. Mater. Interfaces* **2017**, 9, 20255–20275.

(17) Laurier, K. G. M.; Vermoortele, F.; Ameloot, R.; De Vos, D. E.; Hofkens, J.; Roeffaers, M. B. J. Iron(III)-based metal-organic frameworks as visible light photocatalysts. *J. Am. Chem. Soc.* **2013**, 135, 14488–14491.

(18) Qiu, J. H.; Zhang, X. G.; Feng, Y.; Zhang, X. F.; Wang, H. T.; Yao, J. F. Modified metal-organic frameworks as photocatalysts. *Appl. Catal. B* **2018**, 231, 317−342.

(19) Steinebrunner, D.; Schnurpfeil, G.; Kohröde, M.; Epp, A.; Klangnog, K.; Tapia Burgos, J. A.; Wichmann, A.; Wöhrle, D.; Wittstock, A. Impact of photosensitizer orientation on the distance dependent photocatalytic activity in zinc phthalocyanine-nanoporous gold hybrid systems. *RSC Adv.* **2020**, 10, 23203−23211.

(20) Bao, Y. L.; Yu, H. Y.; Zhang, Y.; Chen, L. Comparative study of two poly(amino acid)-based photosensitizer-delivery systems for photodynamic therapy. *Int. J. Biol. Macromol.* **2021**, 169, 153−160.

(21) Mack, J.; Kobayashi, N. Low symmetry phthalocyanines and their analogues. *Chem. Rev.* **2011**, 111, 281−321.

(22) Ke, M. R.; Huang, J. D.; Weng, S. M. Comparison between non-peripherally and peripherally tetra-substituted zinc(II) phthalocyanines as photosensitizers: synthesis, spectroscopic, photochemical and photobiological properties. *J. Photochem. Photobiol. A* **2009**, 201, 23−31.

(23) Haruhiko, T.; Shojiro, S.; Shinsaku, S. Synthesis of metallophthalocyanines from phthalonitrile with strong organic bases. *Chem. Lett.* **1983**, 12, 313−316.

(24) Metz, J.; Schneider, O.; Hanack, M. Synthesis and properties of substituted (phthalocyaninato)-iron and -cobalt compounds and their pyridine adducts. *Inorg. Chem.* **1984**, 23, 1065−1071.

(25) Kantekin, H.; Yalazan, H.; Kahriman, N.; Ertem, B.; Serdaroğlu, V.; Pişkin, M.; Durmuş, M. New peripherally and non-peripherally tetra-substituted metal-free, magnesium(II) and zinc(II) phthalocyanine derivatives fused chalcone units: design, synthesis, spectroscopic characterization, photochemistry and photophysics. *J. Photochem. Photobiol. A* **2018**, 361, 1−11.

(26) Köksoy, B.; Durmuş, M.; Bulut, M. Tetra- and octa-[4-(2-hydroxyethyl)phenoxy bearing novel metal-free and zinc(II) phthalocyanines: synthesis, characterization and investigation of photophysicochemical properties. *J. Lumin.* **2015**, 161, 95−102.

(27) Hu, Z. H.; Tao, C. A.; Liu, H. P.; Zou, X. R.; Zhu, H.; Wang, J. F. Fabrication of an NH_2-MIL-88B photonic film for naked-eye sensing of organic vapors. *J. Mater. Chem. A* **2014**, 2, 14222−6.

(28) Feng, J. J.; Wang, H. Q.; Ma, Z. F. Ultrasensitive amperometric immunosensor for the prostate specific antigen by exploiting a Fenton reaction induced by a metal-organic framework nanocomposite of type Au/Fe-MOF with peroxidase mimicking activity. *Microchim. Acta* **2020**, 187, 95−8.

(29) Spiller, W.; Kliesch, H.; Wöhrle, D.; Hackbarth, S.; Röder, B.; Schnurpfeil, G. Singlet oxygen quantum yields of different photosensitizers in polar solvents and micellar solutions. *J. Porphyr. Phthalocyanines* **1998**, 2, 145−158.

(30) Entradas, T.; Waldron, S.; Volk, M. The detection sensitivity of commonly used singlet oxygen probes in aqueous environments. *J. Photochem. Photobiol. B* **2020**, 204, 111787−11.

(31) Wu, Z. W.; Chen, C.; Wan, H.; Wang, L.; Li, Z.; Li, B. X.; Guo, Q. R.; Guan, G. F. Fabrication of magnetic NH_2-MIL-88B (Fe) confined brønsted ionic liquid as an efficient catalyst in biodiesel synthesis. *Energy Fuels* **2016**, 30, 10739−10746.

(32) Kockrick, E.; Lescouet, T.; Kudrik, E. V.; Sorokin, A. B.; Farrusseng, D. Synergistic effects of encapsulated phthalocyanine complexes in MIL-101 for the selective aerobic oxidation of tetralin. *Chem. Commun.* **2011**, 47, 1562−1564.

(33) Schwab, M. G.; Fassbender, B.; Spiess, H. W.; Thomas, A.; Feng, X.; Müllen, K. Catalyst-free preparation of melamine-based microporous polymer networks through Schiff base chemistry. *J. Am. Chem. Soc.* **2009**, 131, 7216−7217.

(34) Xu, C. H.; Bao, M. J.; Ren, J. W.; Zhang, Z. G. NH_2-MIL-88B ($Fe_\alpha In_{1-\alpha}$) mixed-MOFs designed for enhancing photocatalytic Cr(vi) reduction and tetracycline elimination. *RSC Adv.* **2020**, 10, 39080−39086.

(35) Li, X. H.; Guo, W. L.; Liu, Z. H.; Wang, R. Q.; Liu, H. Quinone-modified NH_2-MIL-101(Fe) composite as a redox mediator for improved degradation of bisphenol A. *J. Hazard. Mater.* **2017**, 324, 665−672.

(36) Lu, H.; Zhang, H. K.; Wang, J.; Zhou, J. T.; Zhou, Y. A novel quinone/reduced graphene oxide composite as a solid-phase redox mediator for chemical and biological acid yellow 36 reduction. *RSC Adv.* **2014**, 4, 47297−47303.

(37) Steinebrunner, D.; Schnurpfeil, G.; Wichmann, A.; Woehrle, D.; Wittstock, A. Synergistic effect in zinc phthalocyanine-nanoporous gold hybrid materials for enhanced photocatalytic oxidations. *Catalysts* **2019**, 9, 555−14.

(38) Lei, Z. D.; Xue, Y. C.; Chen, W. Q.; Li, L.; Qiu, W. H.; Zhang, Y.; Tang, L. The influence of carbon nitride nanosheets doping on the crystalline formation of MIL-88B(Fe) and the photocatalytic activities. *Small* **2018**, 14, 1802045−8.

(39) Jia, X.; Ye, H. N.; Weng, H. L.; Huang, N.; Yu, Y.; Xue, J. P. Small molecular target-based multifunctional upconversion nanocomposites for targeted and in-depth photodynamic and chemo-anticancer therapy. *Mater. Sci. Eng. C* **2019**, 104, 109849−8.

(40) Dhami, S.; Phillips, D. Comparison of the photophysics of an aggregating and non-aggregating aluminium phthalocyanine system incorporated into

unilamellar vesicles. *J. Photochem. Photobiol. A* **1996**, 100, 77–84.

(41) Li, M.; Sun, W.; Tian, R. S.; Cao, J. F.; Tian, Y.; Gurram, B.; Fan, J. L.; Peng, X. J. Smart J-aggregate of cyanine photosensitizer with the ability to target tumor and enhance photodynamic therapy efficacy. *Biomaterials* **2021**, 269, 120532–12.

(42) Zhang, X. F.; Guo, W. F. Indole substituted zinc phthalocyanine: improved photosensitizing ability and modified photooxidation mechanism. *J. Photochem. Photobiol. A* **2011**, 225, 117–124.

(43) Wang, Y. X.; Zhong, Z.; Muhammad, Y.; He, H.; Zhao, Z. X.; Nie, S. X.; Zhao, Z. X. Defect engineering of NH_2-MIL-88B (Fe) using different monodentate ligands for enhancement of photo-Fenton catalytic performance of acetamiprid degradation. *Chem. Eng. J.* **2020**, 398, 125684–12.

(44) Zhou, Y. Z.; Zhang, Y. C.; Li, Z. L.; Hao, C. T.; Wang, Y.; Li, Y.; Dang, Y.; Sun, X. Q.; Han, G. P.; Fu, Y. L. Oxygen reduction reaction electrocatalysis inducing Fenton-like processes with enhanced electrocatalytic performance based on mesoporous ZnO/CuO cathodes: treatment of organic wastewater and catalytic principle. *Chemosphere* **2020**, 259, 127463–12.

(45) Li, Y. Z.; Huangfu, C.; Du, H. J.; Liu, W. B.; Li, Y. W.; Ye, J. S. Electrochemical behavior of metal-organic framework MIL-101 modified carbon paste electrode: an excellent candidate for electroanalysis. *J. Electroanal. Chem.* **2013**, 709, 65–69.

(46) Maruthupandy, M.; Muneeswaran, T.; Anand, M.; Quero, F. Highly efficient multifunctional graphene/chitosan/magnetite nanocomposites for photocatalytic degradation of important dye molecules. *Int. J. Biol. Macromol.* **2020**, 153, 736–746.

(47) Zhao, H. M.; Zhang, T. T.; Shan, D. Y.; Zhu, Y.; Gao, G.; Liu, Y.; Liu, J.; Liu, M. Y.; You, W. S. $ZnIn_2S_4/In(OH)_3$ hollow microspheres fabricated by one-step l-cysteine-mediated hydrothermal growth for enhanced hydrogen production and MB degradation. *Int. J. Hydrog. Energy* **2020**, 45, 13975–13984.

(48) Xing, R.; Wu, P.; Wu, L.; Fei, Z. H. Mesopolymer modified with palladium phthalocyaninesulfonate as a versatile photocatalyst for phenol and bisphenol a degradation under visible light irradiation. *J. Environ. Sci.* **2013**, 25, 1687–1695.

(49) Daneshvar, H.; Seyed Dorraji, M. S.; Amani-Ghadim, A. R.; Rasoulifard, M. H. Enhanced sonocatalytic performance of ZnTi nano-layered double hydroxide by substitution of Cu(II) cations. *Ultrason. Sonochem.* **2019**, 58, 104632–9.

(50) Jorfi, S.; Kakavandi, B.; Motlagh, H. R.; Ahmadi, M.; Jaafarzadeh, N. A novel combination of oxidative degradation for benzotriazole removal using TiO_2 loaded on $Fe^{II}Fe_2^{III}O_4$@C as an efficient activator of peroxymonosulfate. *Appl. Catal. B* **2017**, 219, 216–230.

(51) Kavitha, M. K.; Pillai, S. C.; Gopinath, P.; John, H. Hydrothermal synthesis of ZnO decorated reduced graphene oxide: understanding the mechanism of photocatalysis. *J. Environ. Chem. Eng.* **2015**, 3, 1194–1199.

(52) Zhang, Z. C.; He, D. Y.; Liu, H. Y.; Ren, M.; Zhang, Y. N.; Qu, J.; Lu, N.; Guan, J. N.; Yuan, X. Synthesis of graphene/black phosphorus hybrid with highly stable P–C bond towards the enhancement of photocatalytic activity. *Environ. Pollut.* **2019**, 245, 950–956.

(53) Ochsner, M. Photophysical and photobiological processes in the photodynamic therapy of tumours. *J. Photochem. Photobiol. B* **1997**, 39, 1–18.